



The best of HST

N. Panagia^{1,2,3,4}

- ¹ Space Telescope Science Institute, 3700 San Martin Drive, Baltimore, MD 21218, USA
- ² Istituto Nazionale di Astrofisica – Osservatorio Astrofisico di Catania, Via S. Sofia 78, I-95123 Catania, Italy
- ³ International Center for Relativistic Astrophysics, Piazza della Repubblica 10, I-65122 Pescara, Italy
- ⁴ Supernova Ltd, OYV #131, Northsound Road, Virgin Gorda, British Virgin Islands.
e-mail: panagia@stsci.edu

Abstract. I summarize the current status of the Hubble Space Telescope (*HST*) and illustrate some of its most interesting results.

Key words. Telescopes: HST – Space Vehicles: Instruments – Cosmology: observations – Distance Scale – Cosmological Parameters – Dark Matter – Early Universe – Gamma-Ray Bursts: Host Galaxies – Local Group – Galaxies: halos – Supernovae: 1987A – Stars: V838 Mon – Planetary Systems – Comet: SL9 – Planets and Satellites: Jupiter

1. Introduction

After nineteen years in orbit, the “middle-aged” Hubble Space Telescope (*HST*) continues to play a major role in astronomical research, and is undoubtedly one of the most important and most prolific space astronomy missions of all time.

HST was deployed in low-Earth orbit (about 600 km) by the crew of the space shuttle Discovery (STS-31) on 25 April 1990. Although at the beginning the mission looked severely faulted because of spherical aberration, the first maintenance mission (STS-61 Endeavour, December 1993) fully restored the functionality of *HST*. In fact, all *HST* servicing missions so far, namely SM1 in December 1993, SM2 in February 1997, SM3A in December 1999, and SM3B in February-March 2002 were enormous successes.

Send offprint requests to: N. Panagia

After SM3B, *HST*'s science instruments included a spectrograph, the Space Telescope Imaging Spectrograph (STIS) operating in the UV and optical domains, and three cameras, the Wide Field - Planetary Camera 2 (WFPC2), the new Advanced Camera for Surveys (ACS), which with its tenfold increase in efficiency and its doubled field of view relative to WFPC2 opened up much anticipated new capabilities for discovery, the Near Infrared Camera - Multiobject Spectrograph (NICMOS), which was revived in mission 3B with the installation of a mechanical cooling system, and the Fine Guidance Sensors (FGS, primarily used for astrometric observations).

However, STIS stopped operations in August 2004, leaving *HST* without a proper spectrographic capability, and ACS failed in January 2007, leaving in operation rather old instruments. Subsequently, *HST* suffered a serious malfunction on September 27, 2008, with

a failure of the Side-A Control Unit/Science Data Formatter (CU/SDF) inside the Science Instrument/Control & Data Handling (SI C&DH) system. This prevented data from the science instruments being transmitted to the ground. Data from the Fine Guidance Sensors (FGS) are not routed through the CU/SDF, so *HST* maintained FGS science observations throughout this period. On October 15, *HST* switched to operations on Side B of the CU/SDF, and later resumed science observations with Wide-Field Planetary Camera 2 (WFPC2) and the Advanced Camera for Surveys Solar Blind channel (ACS/SBC).

2. The Servicing Mission 4 gives new life to HST

With more than 19 years of historic and trail-blazing science already accomplished, Hubble has been reborn with the Servicing Mission 4 (SM4). The mission has featured the installation of two new cutting-edge science instruments to enhance Hubble's capabilities by large factors, the refurbishment of Hubble's subsystems and extension of operating life to at least 2014. Astronauts also have succeeded in the first ever on-orbit repair of two existing instruments - both STIS and ACS.

Originally, SM4 was planned for 2004, but was postponed after the Columbia Space Shuttle tragedy in 2003 and then canceled in light of Agency safety concerns. Following the successful recovery of the Shuttle program and a re-examination of SM4 risks, NASA approved one last servicing mission. The reinstated SM4 was initially scheduled for flight in Fall 2008, but after the failure of Side-B CU/SDF it was postponed to late Spring 2009.

On May 11, 2009, SM4 (STS125) started triumphally with the shuttle Atlantis taking seven astronauts to reach the HST, do all repairs and new installations on the telescope in five very intense EVA (ExtraVehicular Activity) sessions, and come back safely on May 24, 2009.

The new instruments are the Cosmic Origins Spectrograph and the Wide Field Camera 3. A refurbished Fine Guidance Sensor has replaced one degrading unit of three now

onboard, and will maintain a robust ability to point the telescope. Astronauts also installed gyros, batteries and thermal blankets to ensure Hubble functions efficiently for a minimum of five, and possibly ten years after servicing.

2.1. New instruments

Cosmic Origins Spectrograph, or COS, is the most sensitive ultraviolet spectrograph ever flown on Hubble. In particular, a factor more than 30 times greater than that of previous spectroscopic instruments in the far-ultraviolet channel and two-fold enhancement in the near-ultraviolet channel.

Wide Field Camera 3, or WFC3, spans the electromagnetic spectrum from the near ultraviolet through the optical, and into the near infrared. WFC3's "UVIS" detector - sensitive to near ultraviolet and optical light - will provide a 35 times improvement in discovery efficiency in near ultraviolet and blue light. The near infrared detector will provide a 15-20 times improvement in discovery efficiency over the current NICMOS instrument.

The new **Fine Guidance Sensor**, or FGS, will extend the life of Hubble's "pointing control system," of which three FGS's are a key component.

2.2. Subsystem components

Gyroscopes - With SM4 a fresh set of six new gyros have been installed to make the most of Hubble's new science instruments and lifetime peak performance through 2013.

Battery Modules - The replacement of the two Hubble battery modules (each containing three batteries) has rejuvenated the electrical power system. This, combined with the power system enhancements made in Servicing Mission 3B, will result in ample power margins for the remainder of Hubble's lifetime.

New Outer Blanket Layer - Stainless steel sheets are slated to be installed on Hubble's exterior to provide additional thermal protection to some equipment bays, replacing the existing multilayer insulation which has slowly de-

graded over time due to the harsh environment of space.

2.3. Repairs and a future rendezvous

Space Telescope Imaging Spectrograph - STIS, the most versatile spectrograph ever to fly on Hubble, has been resuscitated thanks to an on-orbit replacement of a failed electronics board inside one of its main electronics boxes. COS and STIS are highly complementary and would work effectively together to provide a full set of spectroscopic tools for astrophysical research.

Advanced Camera for Surveys - Astronauts have successfully repaired the Advanced Camera for Surveys by replacing the CCD electronics box in the Wide Field Channel and power this box with a replacement low voltage power supply. Thus, ACS will again provide the most sensitive images available at visible and near-infrared wavelengths.

Soft Capture Mechanism - The SCM is a compact device that, when attached to the Hubble aft bulkhead, will enable and assist in the safe de-orbiting of the Hubble Space Telescope at the end of its useful life. This circular mechanism has structures and targets that will allow a next-generation vehicle to more easily capture and guide the telescope into a safe controlled re-entry.

3. *HST* results

In 19 years *HST* has made almost 900,000 observations, obtaining almost 500,000 images of about 30,000 different fields.

Observations made with the *HST* have either solved problems that had been under debate for many years, or have revealed quite unexpected and exciting new phenomena. Among the *HST* high impact science we can mention the definitive measurement of the expansion rate of the Universe, the so-called Hubble constant, the confirmation and characterization of massive black holes in the centers of galaxies, the detection of the host galaxies of QSOs, and the exhaustive study of the properties of the intergalactic medium that tell us about the chemical evolution of the

Universe. Even more exciting are the discoveries that were totally unanticipated and that have opened new avenues to our knowledge of the cosmos, such as the discovery of the acceleration of the Universe, which may imply the existence of the so-called “dark energy” that has been dominating the expansion of the Universe in the last 8 billion years (*e.g.*, Panagia 2005a), the properties of extremely distant galaxies as shown by the Hubble Deep Fields, as well the Hubble Ultra-Deep Field observations that have provided us the direct view at thousands of galaxies formed just a few hundred million years after the Big Bang, clues to the nature of gamma-ray burst sources that are possibly the most energetic explosions in the Universe, the formation of planets in disks around young stars, the full characterization of planets orbiting around other stars but our own Sun, and the dramatic collision of comet Shoemaker-Levy 9 fragments with Jupiter’s atmosphere.

With so many exciting results, one should write a thick book to do justice to all of them and to the other many important discoveries that *HST* has enabled us to make. Here, I shall highlight some of the most impressive discoveries made possible by Hubble. Summaries of previous years most exciting *HST* results may be found in Panagia (1999, 2002, 2004, 2005b).

4. Cosmology and the distant Universe

4.1. High redshift Type Ia supernovae and the acceleration of the Universe

Since supernovae are very bright objects and are relatively common (in an “average cluster of galaxies” with, say, $10^{13} M_{\odot}$ in stars, one may expect several SN explosions to occur per year), they constitute prime candidates to probe distances to galaxies.

That Type Ia supernovae (SNIa) could be used as standard candles has been proposed for many years. However, most of the progress in this field has occurred over the last two decades. Extensive ground-based surveys have identified a large number of new supernovae and characterized their global properties in

a statistically meaningful way. At the same time, using the Hubble Space Telescope, a team led by Sandage has carried out an extensive program to determine the absolute brightness of a selected sample of supernovae (*e.g.*, Sandage *et al.* 2006 and references therein). This has allowed to place the Hubble diagram for SNIa on an absolute scale and the Hubble constant itself to be determined with a precision better than 10%. In particular, they derived a value for the Hubble constant of $H_0 = 62.3 \pm 1.3(\text{statistical}) \pm 5.0(\text{systematic}) \text{ km s}^{-1} \text{ Mpc}^{-1}$. A similar study done by the so-call H_0 Key Project (Freedman *et al.* 2001) led to a higher value obtained using SNIa as standard candles, namely $H_0(KP) = 71 \pm 2(\text{statistical}) \pm 6(\text{systematic}) \text{ km s}^{-1} \text{ Mpc}^{-1}$. In both cases the main source of uncertainty (about 8%) arises from systematic errors, mostly due to the calibration of the period-luminosity relation of Cepheids. The two determinations are not significantly different from each other, and it makes sense to combine them to obtain a “compromise” value which is consistent with both studies, *i.e.* $\langle H_0 \rangle = 65 \pm 5 \text{ km s}^{-1} \text{ Mpc}^{-1}$. This value implies possible ages of the Universe in the range 11-17 *Gyrs*, depending of the acceleration/deceleration history of the Universe itself.

Once the expansion rate is determined, the next step is to determine its variation in the course of the evolution of the Universe, *i.e.* the derivative of its expansion rate. It is interesting to note that, since one wants to measure the derivative of the expansion rate, it is only necessary to verify that SNe Ia are indeed standard candles, *i.e.* they have the same properties at all redshifts (or, equivalently, at all look-back times), with no need to determine their absolute luminosities. In other words, one could measure the acceleration parameters without measuring H_0 , and viceversa.

The acceleration of the Universe can be determined using SNIa as standard candles, if these are observed at suitably large distances in order to reveal a measurable deviation from a constant expansion. Moreover, Goobar and Perlmutter (1995) showed the possibility of separating the relative contributions of the

mass density, Ω_M , and the cosmological constant, Λ (or, equivalently, its dimensionless parameter $\Omega_\Lambda = \Lambda/3H_0^2$), to changes in the expansion rate by studying supernovae at a range of redshifts.

Pioneering work by Danish astronomers (Nørgaard-Nielsen *et al.* 1989) led to the discovery of one SNIa at $z = 0.31$ as the result of a multi-year observational effort. It was only when Perlmutter’s Supernova Cosmology Project (SCP) took off that SNIa searches at high redshifts became an efficient reality. Thanks to their use of large format CCDs, a clever observational strategy, and sophisticated image analysis techniques, in 1992 they discovered their first high redshift SNIa, SN 1992bi at $z = 0.46$ (Perlmutter *et al.* 1995), followed in 1994 by 6 more at $z > 0.35$ (Perlmutter *et al.* 1997). Friendly competition promptly followed suit, when the High-Z Supernova Search Team (Schmidt *et al.* 1998) started their systematic searches in 1995, essentially adopting Perlmutter’s strategy and, consistently, also discovering a dozen supernova candidates per run. By mid-1998 the SCP team has discovered and studied about 78 SNIa, most of which in the redshift range 0.2–0.8, and the HZSS team has discovered about 32 SNIa.

The results for a first subset (42 out of 78) of the SCP sample of SNIa was presented and discussed by Perlmutter *et al.* (1999). The best fit confidence regions in the Ω_M – Ω_Λ plane showed that neither an empty Universe ($\Omega_M = 0$, $\Omega_\Lambda = 0$), nor a non-inflationary Universe ($\Omega_\Lambda = 0$) are consistent with the data. For a flat cosmology ($\Omega_M + \Omega_\Lambda = 1$), one would find $\Omega_M^{flat} = 0.24 \pm 0.08$ and $\Omega_\Lambda^{flat} = 0.76 \pm 0.08$. Similar results, but still with a somewhat larger uncertainty, have also been found by the HZSS team from the analysis of 10 of their high z SNIa (Riess *et al.* 1998).

In more recent years, the observers augmented their SNIa samples and routinely complementing their ground-based observations with higher quality photometry obtained with the *HST*–*WFPC2* (*e.g.*, Perlmutter *et al.* 1998). The obvious improvement provided by the superior angular resolution of *HST* is that contamination by the host galaxy light is signif-

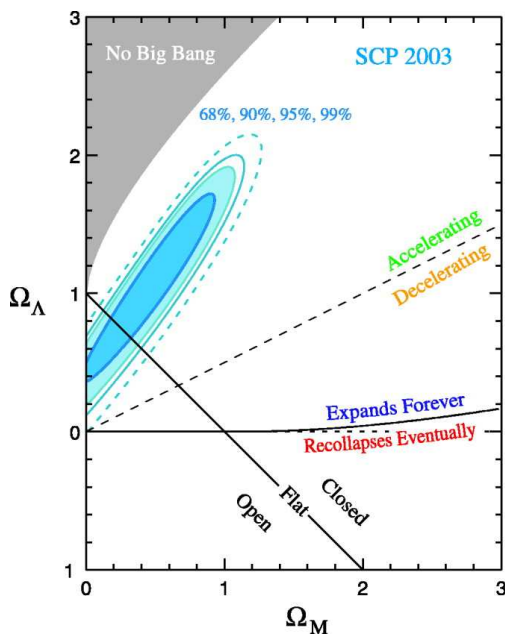


Fig. 1. Constraints to the matter density, Ω_M , and the vacuum energy density, Ω_Λ , as derived from high quality SNIa observations up to $z \sim 0.9$ (Knop *et al.* 2003). The 68%, 90%, 95%, and 99% confidence regions are denoted.

icantly reduced and becomes an easily treatable problem, thus providing higher photometric accuracy.

Over the years the SNIa constraints on Ω_M and Ω_Λ have been tighten up thanks to the superior accuracy and reliability of *HST* photometry, especially with the installation of the ACS. Figure 1 show the results obtained by the SCP studying 11 new SNIa up to $z \sim 0.9$ (Knop *et al.* 2003).

Another quantum leap occurred when high z SNIa searches were carried out in coordination with projects doing very deep imaging to study the nature and the properties of very distant galaxies (*e.g.*, the GOODS project, Giavalisco *et al.* 2004).

In this way Riess *et al.* (2004, 2007) were able to discover 23 SNIa at redshifts greater than 1, to confirm their nature by spectroscopy with the ACS grism, and to monitor their light curves. Their measurements showed that SNIa at redshifts less than 1 appeared to be fainter

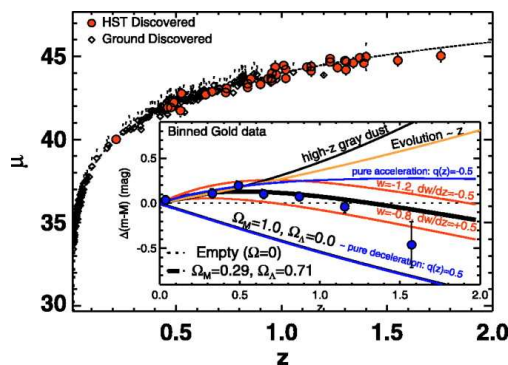


Fig. 2. SN Ia Hubble diagram as obtained by Riess *et al.* (2007). High quality points for SNe Ia from ground-based discoveries are shown as diamonds, HST-discovered SNe Ia are shown as filled symbols. Overplotted is the best fit for a flat cosmology: $\Omega_M = 0.29$, $\Omega_\Lambda = 0.71$. The inset shows the residual Hubble diagram and models relative to an empty Universe model.

than expected for an empty Universe expansion and that, viceversa at higher redshifts they were brighter than the predictions for an empty Universe (see Fig 3). These results are perfectly consistent with the hypothesis of a cosmological constant whose effects are negligible in the early Universe, where the the gravitational deceleration dominates over its constant acceleration, but become dominant when the gravitational effects decrease at lower redshifts. In other words, Type Ia supernovae at $z > 1$ were able to provide the first statistically “convincing” evidence for cosmic deceleration that preceded the current epoch of cosmic acceleration.

However, it is a little distressing to notice that there is a rather large intrinsic dispersion of the SNIa magnitudes around the average relationship corresponding to the concordance cosmology ($\Omega_M \sim 0.29$, $\Omega_\Lambda \sim 0.71$) with $w = -1$ (see Fig 4). We see that the rms deviation is about 0.2 magnitudes which is larger than the maximum systematic “acceleration” effect detectable at $z \sim 0.5$. Although a number of possible phenomena that may produce systematic deviations have been ruled out (such as grey extinction in the IGM or intrinsic luminosity of SNIa monotonically evolving with time), the

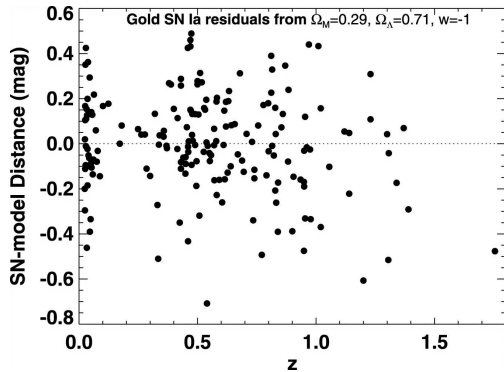


Fig. 3. Distance difference in magnitudes for all high quality SNe ($cz > 7000 \text{ km s}^{-1}$) between the measured distance and that predicted for the concordance cosmology ($\Omega_M \sim 0.29$, $\Omega_\Lambda \sim 0.71$) with $w = -1$. [Adapted from Riess *et al.* 2007]

recent evidence that SNIa may be produced by a multiplicity of progenitors with widely different origins and properties (*e.g.*, Mannucci *et al.* 2005, 2006) makes the case of using SNIa as reliable standard candles much less tight than it would be desirable.

In particular, in the local Universe, SNIa occurring in late type galaxies have been found to be systematically brighter by several tenths of a magnitude than SNIa occurring in early type galaxies (Filippenko 1989, Della Valle & Panagia 1992, Hamuy *et al.* 1996, Howell 2001). Extending this trend to all redshifts, one would predict the alarming effect that SNIa at redshifts less than 0.5-1 would be *intrinsically* dimmer than SNIa occurring at higher redshifts, $z > 1$, which is just the behaviour that is regarded as proof for acceleration. This is a crucial aspect that must be clarified and that requires many more studies and a lot of caution before reaching the “ultimate” conclusion about the reality and the strength of the cosmological acceleration.

4.2. Dark matter

A powerful collision of galaxy clusters has been captured by Hubble Space Telescope and Chandra X-ray Observatory (see Figure 4). The observations of the cluster known as MACS J0025.4-1222 indicate that a titanic col-

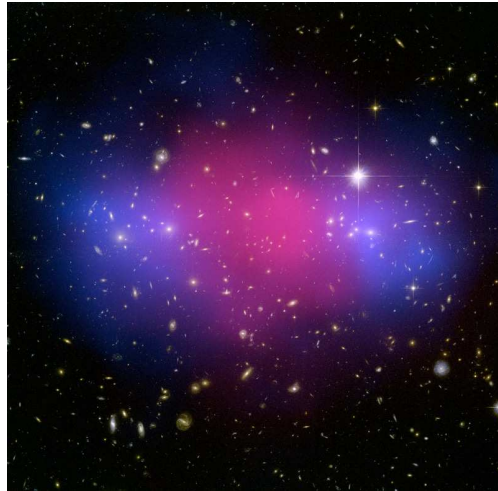


Fig. 4. *HST*-ACS and Chandra composite image of the Galaxy Cluster MACS J0025.4-1222 showing the distributions of ordinary matter (in red (around the cluster center), as mapped by its X-ray emission) and dark matter (in blue (on both sides relative to the center), detected by means of gravitational lensing measurements). [Credit: Bradac & Allen, NASA, ESA, CXC]

lision has separated the dark from ordinary matter (Bradac *et al.* 2008) and provide an independent confirmation of a similar effect detected previously in a target dubbed the Bullet Cluster (1E0657-56, Clowe *et al.* 2004, 2006, Bradac *et al.* 2006). These new results show that the Bullet Cluster is not an anomalous case. This beautiful view of the galaxy cluster MACSJ0025 demonstrates how ordinary matter and mysterious dark matter interact. The blue cloud-shaped parts flanking the centre show the position of dark matter, mapped by *HST*-ACS using gravitational lensing to measure the amount of dark matter. The red middle indicates ordinary matter, charted by NASA’s Chandra X-Ray Observatory. The position of the two matter types shown in the image are explained by MACSJ0025’s origin. It was formed when a pair of large galaxy clusters collided. Ordinary matter in the form of hot gas slowed down and pooled at the centre but dark matter passed straight through.

4.3. The evolution of galaxies and the cosmic star formation rates

The Hubble Deep Field observations, made with the WFPC2 in selected pointings of the Northern and the Southern hemispheres (Williams *et al.* 1996, 2000) opened the way to the study of *really* high redshift galaxies, namely as high as $z \sim 5$ and just about 1.5 billion years after the Big Bang.

The original Northern hemisphere HDF revealed a population of small, irregular galaxies that often appeared in pairs or small groups. Much of the light from these objects was of high surface brightness, owing to high rates of star formation, but concentrated, requiring the resolution of HST to identify them as distant galaxies as opposed to red stars, for example. The extension of the deep-field approach to the southern hemisphere (Williams *et al.* 2000) confirmed the main conclusions of the HDF but also showed the limitations of a small field survey in drawing broad conclusions about distant populations, *i.e.* cosmic error within small fields can be substantial.

With the installation of a more efficient camera, the ACS, deeper and deeper studies were pursued, reaching with the Hubble Ultra Deep Field (HUDF) survey objects at redshifts as high as ~ 7 (Beckwith *et al.* 2006, Mobasher *et al.* 2005).

The ACS Hubble Ultra Deep Field (HUDF) was a public survey, a 1 million s exposure of an 11 square-arcmin region in the southern sky imaged with the ACS on the HST using Director's Discretionary Time. The main science driver was galaxy evolution and cosmology, including probing the epoch of reionization up to $z \sim 6.5$ and characterizing not only the colors but also the morphologies of faint sources. The primary instrument was ACS, but WFPC2, NICMOS and STIS were also used in parallel.

The HUDF consists of a single ultra-deep field (412 orbits in total) within the Chandra Deep Field South (Giacconi *et al.* 2002) in the GOODS area (Giavalisco *et al.* 2004). The adopted pointing was selected so as to avoid the gaps with the lowest effective exposure on the Chandra ACIS image of CDFS, and was

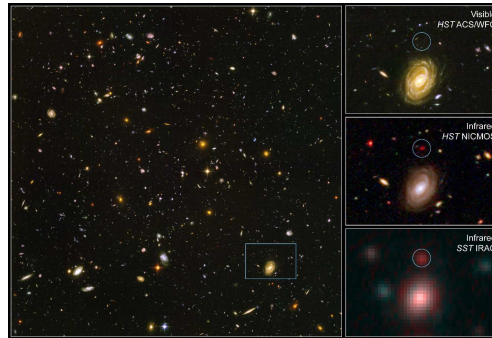


Fig. 5. The Hubble Ultra Deep Field as imaged with the HST-ACS. Also shown are the position, and the corresponding NICMOS and Spitzer-IRAC NIR images (inserts), of the massive galaxy HUDF-JD2, which is estimated to be at a redshift $z \sim 6.5$, the most distant galaxy identified in the HUDF. [Credit: B. Mobasher, NASA, ESA]

designed to include in the field both a spectroscopically confirmed $z=5.8$ galaxy and a spectroscopically confirmed type Ia SN at $z=1.3$. The HUDF field was also selected to be accessible to most major observatories in both Northern and Southern hemispheres.

The ACS exposure time was divided among four filters, F435W (B435), F606W (V606), F775W (i775), and F850LP (z850), to give approximately uniform limiting magnitudes $m_{AB} \sim 29$ for point sources. The HST observations were carried out between late September 2003 and mid-January 2004.

The HUDF field contains at least 10,000 objects, the vast majority of which are galaxies. Three samples of galaxies in different redshift intervals were identified in the HUDF from objects with missing flux in the shortest wavelength bands, those that "dropped out" of the B435, V606, or i775 filters, corresponding approximately to redshift ranges $3.5 < z < 4.7$, $4.6 < z < 5.5$, and $5.7 < z < 7$, respectively. The main findings can be summarized as (Beckwith *et al.* 2006):

- As found in previous observations with the Hubble Space Telescope, galaxies at these high redshifts are smaller and less symmetric in shape than galaxies at lower redshifts. These results confirm that galaxies evolved rapidly in the first few billion years after the Big Bang.

- The faint sources detected by the HUDF are smaller on average than the brighter objects seen in shallower surveys such as GOODS (Giavalisco *et al.* 2004) or the HDFs (Williams *et al.* 1996, 2000), with typical sizes (radius enclosing 50% of the flux) of about 0.15 arc-sec.
- The comoving volume density of galaxies needed to fit these high-redshift samples is at least 10 times smaller than the local value of 0.016 Mpc^{-3} using the simplest assumptions about source selection and the entire comoving volumes allowed by color selection. However, since it is quite likely that the Lyman break dropout technique picks up only a fraction of the galaxies at high redshift, the density derived here may be a lower limit.
- Although the luminosity density of galaxies at wavelengths of 1400 \AA decreases modestly from redshifts of a few out to redshifts greater than 6, vigorous star formation was already underway when the Universe was less than 1 billion years old.

After the installation of WFC3 in mid-May, the HUDF09 program (GO-11563) devoted 192 orbits to observations of three fields, including the HUDF, using the newly available F105W, F125W and F160W near-infrared filters (which correspond to the Y, H and J bands).

In particular, Bouwens *et al.* (2009) used a two-color Lyman-Break selection technique to identify $z \sim 8 - 8.5$ Y-dropouts, and found 5 probable candidates. The sources have H-band magnitudes of ~ 28.5 AB mag, apparent sizes of $\sim 0.15''$ ($\sim 0.7h^{-1}$ kpc), and very blue UV-continuum slopes (*i.e.* $\beta < -2.5$), suggesting that these $z \sim 8$ galaxies are not only dust free but also perhaps have very young ages or low metallicities. The observed number of Y-dropout candidates is smaller than the 21 and 10 sources expected assuming no evolution from $z \sim 6$ and $z \sim 7$, respectively, but is consistent with the 7 expected extrapolating Bouwens *et al.* (2008) luminosity function results to $z \sim 8$.

Deep field observations are also planned for the James Webb Space Telescope later in the mid-2010's.

4.4. Gamma ray bursts

Gamma-ray burst sources (GRBs) are powerful flashes of gamma rays associated with energetic explosions in distant galaxies, and may be the most luminous events occurring in the Universe. The initial burst is usually followed by a longer-lived "afterglow" emitting at longer wavelengths (X-ray, ultraviolet, optical, infrared, and radio). Most observed GRBs are believed to be a narrow beam of intense radiation released during a supernova event, as a rapidly rotating, high-mass star collapses to form a black hole (see *e.g.*, Della Valle 2009)

As summarized by Fruchter *et al.* (2006) when massive stars exhaust their fuel, they collapse and often produce the extraordinarily bright explosions known as core-collapse supernovae. On occasion, this stellar collapse also powers an even more brilliant relativistic explosion known as a long-duration gamma-ray burst. Within this frame, long gamma-ray bursts and core-collapse supernovae should be found in similar galactic environments. Fruchter *et al.* (2006), on the basis an HST-WFPC2 study of about 20 host galaxies long gamma-ray bursts, argue that this is not the case. Actually, they find that GRBs are far more concentrated in the very brightest regions of their host galaxies than are the bulk of core-collapse SNe (see Fig. 6). Moreover, the host galaxies of the long GRBs appear to be fainter and more irregular than the host galaxies of most core-collapse SNe. From these results they conclude that long-duration gamma-ray bursts must be associated with the most extremely massive stars and may be restricted to galaxies of limited chemical evolution.

5. The local Universe

5.1. Stellar populations in nearby galaxies: younger stars in the Andromeda halo?

With an investment of 120 orbits of *HST* observing time, a team led by Tom Brown has obtained a color-magnitude diagram (CMD) for a minor-axis field in the halo of the Andromeda galaxy (M31), 51 arcmin (11 kpc) from the

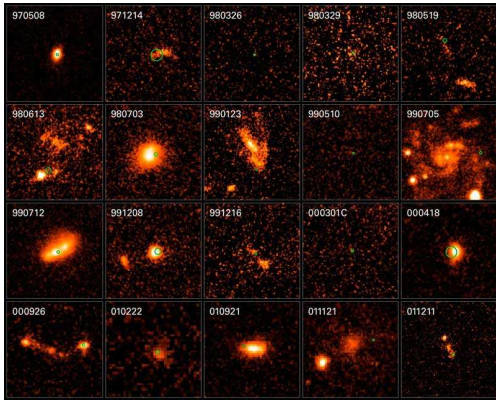


Fig. 6. The host galaxies of 20 long-duration GRB sources as imaged with *HST*. [Credit: NASA, ESA and A.Fruchter (STScI)]

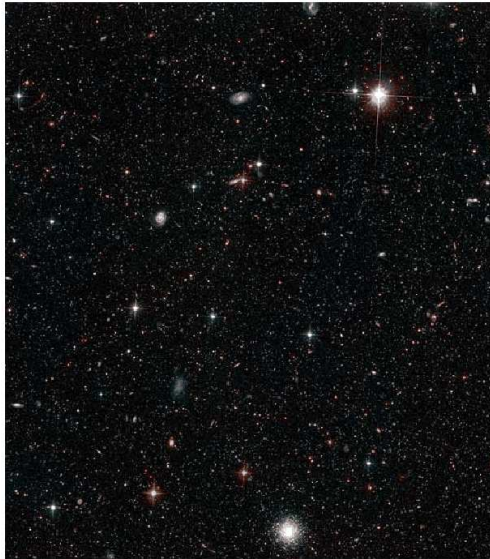


Fig. 7. A $180'' \times 200''$ region of M31 halo, the deepest visible-light image so far taken in space, observed with the *HST-ACS*. [Credit: NASA, ESA and T.M. Brown (STScI)]

nucleus (Brown *et al.* 2003). These observations, taken with the Advanced Camera for Surveys on the Hubble Space Telescope, are among the deepest optical images yet obtained, attaining 50% completeness at $V = 30.7$ mag

(see Figure 7). The CMD, constructed from approximately 300,000 stars, reaches more than 1.5 mag fainter than the old main-sequence turnoff. Brown *et al.* analysis is based on direct comparisons to *ACS* observations of four globular clusters through the same filters, as well as chi-squared fitting to a finely-spaced grid of calibrated stellar-population models. They find that the M31 halo contains a major (approximately 30% by mass) intermediate-age (6-8 Gyr) metal-rich ($[Fe/H] > -0.5$) population, as well as a significant globular-cluster age (11-13.5 Gyr) metal-poor population.

The newly discovered younger stars in Andromeda's halo are richer in heavier elements than the stars in our Milky Way's halo, or in most of the small dwarf galaxies that surround the Milky Way. Indeed the level of chemical enrichment seen in these younger stars is characteristic of relatively massive galaxies, containing at least a billion stars. On the other hand, since the gas in a young giant galaxy rapidly falls into the disk, it is unlikely that the newly revealed intermediate-age population could be explained by star formation continuing in the halo for more than 6 Gyrs.

Brown *et al.* (2003) argue that a more plausible explanation is a merger with a large satellite galaxy when the Universe was approximately half of its present age, or a series of mergers with smaller satellites. Thus, the resulting halo appears to be a mix of stars originally formed in the halo, disrupted-disk stars, disrupted-satellite stars, and stars formed during one or more mergers. These results open a number of interesting new possibilities, but leave us with the new question "what is the typical halo formation process?" Is it a "violent" one like that we see occurring in Andromeda, or is it as quiescent as found in the halo of our Milky Way galaxy? Only further studies on more galaxies will be able to answer this question properly.

5.2. Fireworks in SN 1987A equatorial ring

Supernova 1987A exploded on 1987 February 23 in the Large Magellanic Cloud. Although *HST* was not yet in orbit when this rare chance

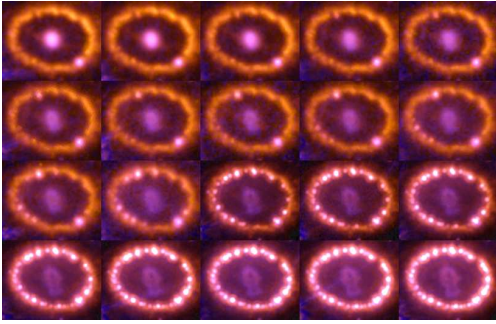


Fig. 8. Series of images of SN 1987A and its inner circumstellar ring obtained with *HST-WFPC2* between late 1994 (top, left) and mid-2006 (bottom, right). It appears that the quiescent ring has developed at least nine hot spots in the last five years. [Courtesy of Peter Challis (CfA), on behalf of the SINS project (Supernova INTensive Study, PI: R.P Kirshner)]

to observe a nearby supernova appeared, it took advantage of the opportunity as soon as it became operational. The European Space Agency's Faint Object Camera took the first images of SN 1987A on 1990 August 23-24, which revealed the supernova crowned by a glorious circumstellar ring. Later, two more rings were discovered.

HST has kept an attentive eye on SN 1987A, and its observations have produced many fundamental results, including a direct measure of the supernova expansion, the detailed properties of its surrounding rings, the accurate measurement of the distance to the supernova, and the origin of the stars associated with the supernova.

Recently, Hubble has observed the high-velocity material from the supernova explosion starting to overtake and crash into the slower-moving inner ring. Figure 8 shows the dramatic evidence of these collisions. The circumstellar ring, which until 1996 was relatively quiescent, started to develop bright spots in 1997, and in mid-2006 one can identify more than twenty bright spots. These bright spots are the result of the fast moving component of the ejecta colliding with the stationary equatorial ring. The fastest debris, moving at $15,000 \text{ km s}^{-1}$ or $1/20$ the speed of light, are now colliding with the slower moving gas which was

ejected when the progenitor was a red supergiant (*e.g.*, Sonneborn *et al.* 1997).

Over the next decades, as “slower” ejecta layers reach the ring, more and more spots will light up and the whole ring will shine as it did in the first several months after explosion. Eventually, the bulk of the ejecta will completely sweep the ring up, clearing the circumstellar space of that remnant of the pre-supernova wind activity.

5.3. The mysterious outburst of the star V838 Monocerotis

The previously unknown variable star V838 Monocerotis erupted in early 2002, brightening suddenly by a factor of almost 10,000 at visual wavelengths. Unlike a supernova or nova, V838 Mon did not explosively eject its outer layers, rather, it simply expanded to become a cool supergiant with a moderate-velocity stellar wind. A series of superluminally expanding ring-like structures appeared around the star shortly afterward, as illumination from the outburst propagated into a surrounding, pre-existing circumstellar dust cloud (see Figure 9). They are produced by simple reflection of light from the star by dust particles that are present in the circumstellar medium and, therefore, they are called “light echoes”. This is the first light echo seen in the Milky Way since 1936. The star and its surrounding medium has been studied through a series of high-resolution images and polarimetry of the light echo with the *HST-ACS*.

The echo exhibits a series of circular arcs, whose angular expansion rates show that the distance is greater than 2 kpc. The polarimetric imaging (Sparks *et al.* 2008) shows that the distance is actually as high as 6 kpc. This distance agrees very well with that measured for the star cluster that surrounds V838 Mon (Afsar & Bond 2007). It is estimated that at maximum light, the object was extremely luminous, at least as bright as visual absolute magnitude -9.6 , which is about a million times brighter than the Sun. The spectrum of the star during the outburst remained that of a cool stellar photosphere, but as the outburst subsided a com-

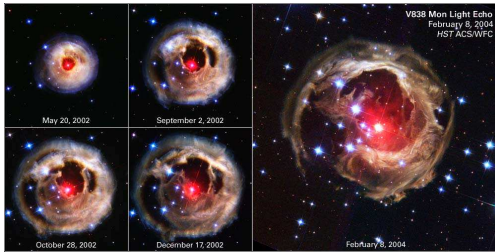


Fig. 9. Comparison of ACS images of V838 Mon obtained between May 20, 2002, and February 8, 2004. The structure is dominated by a series of nearly circular arcs and rings, centered on the variable star, but there are cavities that become progressively more asymmetric with time. [Credit: H.E. Bond (STScI), Hubble Heritage Team, NASA, ESA]

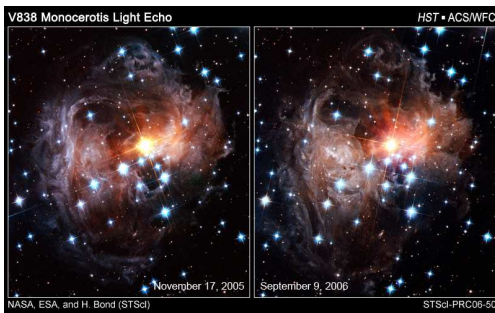


Fig. 10. Comparison of ACS images of V838 Mon obtained between November, 2005, and September, 2006. The apparently slower expansion of the echo may indicate that it has reached the outer layers of the previously ejected material. [Credit: H.E. Bond (STScI), Hubble Heritage Team, NASA, ESA]

posite spectrum appeared, which revealed the presence of a hot star companion.

More recent observations (see Figure 10) show that the expansion of the light echo appears to slow down suggesting that it has reached the outer layers of the previously ejected material. The corresponding radius is about 2 pc, which, adopting a physical expansion velocity similar to the observed velocity of the ejecta in 2002 outburst ($\sim 200 \text{ km s}^{-1}$), provides an age of about 10,000 years for the last matter ejection episode before the 2002 outburst.

V838 Mon thus appears to represent a new class of stellar outbursts, occurring in binary systems containing a relatively hot main-sequence star and a companion that erupts to become a cool supergiant. A remarkably similar event was seen in the Andromeda Galaxy in the late 1980's. The presence of the circumstellar dust implies that previous eruptions have occurred, and spectra show it to be a binary system. When combined with the high luminosity and unusual outburst behavior, these characteristics indicate that V838 Mon represents a hitherto unknown type of stellar outburst, for which we have no completely satisfactory physical explanation.

6. Observations of planets, far and near

6.1. A transiting extrasolar planet

The low mass companion to HD 209458 was the first extrasolar planet found to transit the disk of its parent star (Charbonneau *et al.* 2000, Mazeh *et al.* 2000).

The importance of studying transits of planets in front of their parent star resides in the fact that one can directly determine the size of the planet relative to the star. Since the star radius is known at least from its spectral type, one can obtain an accurate measure of the planet absolute size. Moreover, from measurements of radial velocities of the parent star, which trace the wobble of the star due to the presence of the planet, one can unambiguously determine the planet mass. Having the mass and the size of the orbiting planet, one can derive the average density of the planet, which can put stringent constraints to the theoretical models of planet formation.

HST-STIS observations of the HD 209458 system (see Figure 11) indicated the presence of a companion planet with orbital period of 3.5247 days, a lower limit to its mass of $M_p = 0.70 \pm 0.05 M_J$, a planet radius $R_p = 1.35 \pm 0.06 R_J$ and a separation of 0.00468 AU (Brown *et al.* 2001). A detailed analysis of the transit light curve led to the conclusion that the planet had no rings (which would have appreciably altered the shape of the light curve)

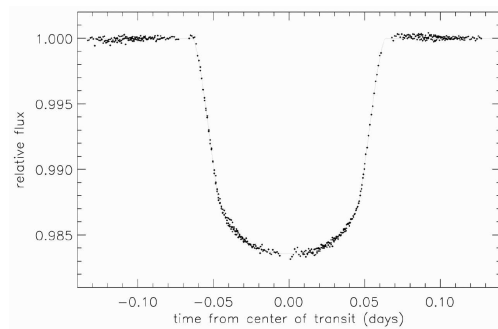


Fig. 11. HD 209458 HST-STIS light curve provides evidence for a planet transit (Brown *et al.* 2001)

nor an orbiting satellite with mass higher than $3M_{Earth}$ (whose presence would have affected the symmetry of the light curve).

On the other hand, spectrophotometric observations made at the time of four transits revealed that the NaI line at 5889\AA absorption line was becoming detectably stronger, *i.e.* $(2.32 \pm 0.57) \times 10^{-4}$, providing clear evidence for the presence of a Na-rich atmosphere in the planet (Charbonneau *et al.* 2001). This is the first detection of an atmosphere in an extrasolar planet that marks the beginning of a new and exciting era in which extrasolar planets begin being fully characterized instead of being merely detected gravitationally as point sources with mysterious properties.

6.2. Carbon compounds discovered on an extrasolar planet

Extensive observations made in May 2007 with Hubble's Near Infrared Camera and Multi-Object Spectrometer (NICMOS) have allowed Swain *et al.* (2008) to detect the presence of methane in the exoplanet HD 189733b, which is orbiting around the K-type dwarf HD 189733. They also were able to confirm the existence of water molecules in the planet's atmosphere, a discovery made originally by NASA's Spitzer Space Telescope in 2007 (Tinetti *et al.* 2007).

The observations were made as the planet transited (Pont *et al.* 2007) in front of its parent star, as illustrated in Fig. 12. As the stellar light passed through the atmosphere along the edge

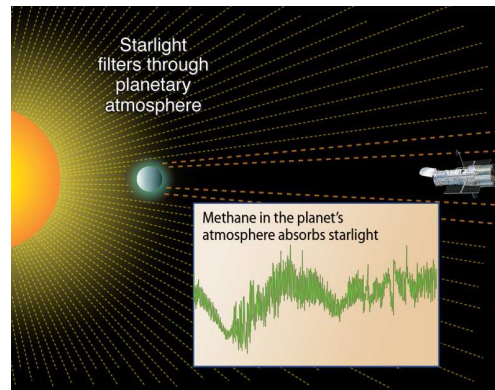


Fig. 12. Artist illustration of the absorption by the edge of the transiting planet's atmosphere. [Credit: A. Feild (STScI), NASA, ESA]

of the planet, the gas in the atmosphere imprinted their unique absorption signatures on the spectrum radiated by the star HD 189733.

More recently (June and August 2008), Swain *et al.* making additional NICMOS observations were also able to detect the presence of both CO_2 and CO in the planet's atmosphere.

Although HD 189733b is too massive and too hot (with a mass of about $1.2 m_{Jupiter}$ and a surface temperature of about 1,300 K it qualifies as a "hot Jupiter") to be a likely host for life, these observations are a proof-of-concept demonstration that the basic chemistry for life can be measured on planets orbiting other stars. The ultimate goal of studies like these is to identify prebiotic molecules in the atmospheres of planets in the "habitable zones" around other stars, where temperatures are right for water to remain liquid rather than freeze or evaporate away.

This successful demonstration of looking at the near-infrared spectrum of the parent star as modified by a planet's atmosphere absorption is very encouraging for astronomers planning to use the James Webb Space Telescope when it is launched in 2013 (see sections 8-10). Since biomarkers are best seen at near-infrared wavelengths, spectroscopy with the JWST will provide an ideal tool to detect biomarkers on a terrestrial planet the size of Earth, or a "super-Earth" several times our planet's mass.



Fig. 13. A composite of several images of Comet P/Shoemaker-Levy 9 fragments taken with HST-WFPC2 in February 1994 that shows the full "string of pearls", i.e. the whole series of the comet fragments [Credit: H.A Weaver & T.E.. Smith (STScI), NASA]

6.3. The impact of comet Shoemaker-Levy 9 on Jupiter

Comet Shoemaker-Levy 9 (SL9, formally designated D/1993 F2) was a comet that broke apart and collided with Jupiter in July 1994, providing the first direct observation of an extraterrestrial collision of solar system objects. The collision provided new information about Jupiter and highlighted its role in reducing space debris in the inner solar system.

In July 1992 the orbit of Shoemaker-Levy 9 had passed within Jupiter's Roche limit, and Jupiter's tidal forces acted to pull the comet apart. SL9 was later observed as a series of fragments ranging up to 2 km in diameter, often referred to as the "string of pearls".

An observing campaign, lead by Heidi Hammel, was launched to study this unique event with Hubble. The twenty-one large chunks of the comet collided with Jupiter's southern hemisphere between July 16 and July 22, 1994, at a speed of approximately 60 km/s. The prominent scars from the impacts were more easily visible than the GreatRed Spot and persisted for many months. In particular, an *HST* image of Jupiter obtained on July 22, 1994, shows eight impact sites (see Fig. 14). From left to right are the E/F complex (barely visible on the edge of the planet), the star shaped H site, the impact sites for tiny N, Q1, small Q2, and R, and on the far right limb the D/G complex. The D/G complex also shows extended haze at the edge of the planet. The features are rapidly evolving on timescales of days. The smallest features in the this image are less than 200 kilometers across.

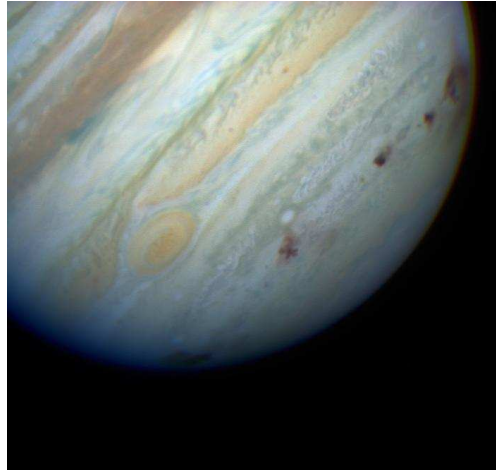


Fig. 14. Image of Jupiter taken with the HST-WFPC2 on July 22, 1994. Eight impact sites are visible [Credit: NASA, ESA, H. Hammel (Space Science Institute, Boulder, Colo.), and the Jupiter Impact Team]

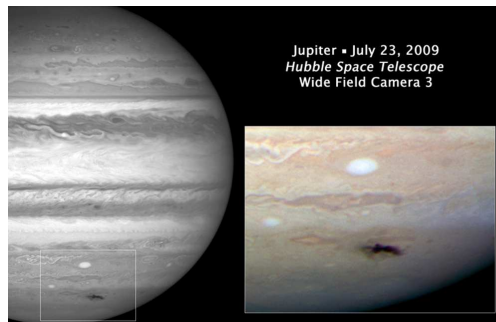


Fig. 15. A new spot on Jupiter, caused by the impact of a comet or an asteroid, was observed with HST-WFC3 on July 23, 2009 [Credit: NASA, ESA, H. Hammel (Space Science Institute, Boulder, Colo.), and the Jupiter Impact Team]

This was the first impact ever observed in the Solar system but not the last one!

On July 23, 2009, NASA scientists interrupted the checkout and calibration of the Hubble Space Telescope to aim at a new expanding spot on Jupiter. The spot, caused by the impact of a comet or an asteroid, was discovered by the Australian amateur astronomer Anthony Wesley on July 19, 2009. The Hubble

picture (Fig. 15), taken on July 23, 2009, is the sharpest image taken of the impact feature.

The observations were made with *HST* new camera, the Wide Field Camera 3. Even if WFC3 was not yet fully calibrated, it is clear that the it is already able to return meaningful science images that can complement images taken with ground-based telescopes.

Acknowledgements. I am grateful with the organizers for inviting me to another very interesting workshop. This work was supported in part by STScI-DDRF Grant D0001.82392, and NASA Grant HST-GO-11217.05A

References

- Afsar, M., & Bond, H.E., 2007, *AJ*, 133, 387
 Beckwith, S.V.W., et al., 2006, *AJ*, 132, 172
 Bond, H.E., et al., 2003, *Nature*, 422, 405
 Bouwens, R.J., et al., 2008, *ApJ*, 686, 230
 Bouwens, R.J., et al., 2009, *astro-ph/0909.1803*
 Bradac, M., et al., 2006, *ApJ*, 652, 937
 Bradac, M., et al., 2008, *ApJ*, 687, 959
 Brown, T.M., et al., 2001, *ApJ*, 552, 699
 Brown, T.M., et al., 2003, *ApJ*, 592, L17
 Clowe, D., et al., 2004, *ApJ*, 604, 596
 Clowe, D., et al., 2006, *ApJ*, 648, L109
 Della Valle, M., Panagia, N., 1992, *AJ*, 104, 696
 Della Valle, M., 2009, in *Probing Stellar Populations out to the Distant Universe: Cefalù 2008*, eds. L.A. Antonelli, E. Brocato, M. Limongi, N. Menci, G. Raimondo, & A. Tornambè, *AIP Conf. Proc. Series*, 1111, 393
 Filippenko, A.V., 1989, *PASP*, 101, 588
 Freedman, W., et al., 2001, *ApJ*, 553, 47
 Fruchter, A. et al., 2006, *Nature*, 441, 463
 Giacconi, et al., 2002, *ApJS*139, 369
 Giavalisco M., et al., 2004, *ApJ*, 600, L93
 Hamuy, M., et al., 2000, *AJ*, 120, 1479
 Howell, D.A., 2001, *ApJ*, 554, L193
 Knop, R.A., et al., 2003, *ApJ*, 598, 102
 Mannucci, F., et al., 2005, *A&A*, 433, 807
 Mannucci, F., Della Valle, M., & Panagia, N., 2006, *MNRAS*, 370, 773
 Mobasher, B., et al., 2005, *ApJ*, 635, 832
 Nørgaard-Nielsen, H.U., et al., 1989, *Nature*, 339, 523
 Panagia N., 1999, in *Frontier Objects in Astrophysics and Particle Physics*, eds. F. Giovannelli & G. Mannocchi, Italian Physical Society (Bologna - Italy), CP Vol. 65, p. 25-36.
 Panagia N., 2002, *Mem. S.A.It.*, 73, 889
 Panagia N., 2004, *ESA Bu.*, 118, 4.
 Panagia N., 2005a, *NCimB*, 120, 667
 Panagia N., 2005b, *NCimB*, 120, 897
 Perlmutter, S., et al., 1995, *ApJ*, 440, 41
 Perlmutter, S., et al., 1997, *ApJ*, 483, 565
 Perlmutter, S., et al., 1998, *Nature*, 391, 51
 Perlmutter, S., et al., 1999, *ApJ*, 517, 565
 Pont, F., et al., 2007 *A&A*, 476, 1347
 Rages K., Hammel H.B., Lockwood G.W., 2002, *Icarus*, 159, 262
 Riess, A.G., et al., 1998, *AJ*, 116, 1009
 Riess, A.G., et al., 2004, *ApJ*, 607, 665
 Riess, A.G., et al., 2007, *ApJ*, 659, 98
 Sandage, A., et al., 2006, *ApJ*, 653, 843
 Schmidt, B.P., et al., 1998, *ApJ*, 507, 46
 Sonneborn, G., et al., 1997, *ApJ*, 477, 848
 Sparks, W.B., et al., 2008, *AJ*, 135, 605
 Sromovsky L.A., Fry P.M., Limaye S.S., Baines K.H., 2003, *Icarus*, 163, 256
 Swain, M.R., Vasisht, G, & Tinetti, G., 2008, *Nature*, 462, 329
 Tinetti, G., et al., 2007, *Nature*, 448, 169
 Williams, R.E., et al., 1996, *AJ*, 112, 1335
 Williams, R.E., et al., 2000, *AJ*, 120, 2735